

Article

# 3D Printed and Embedded Strain Sensors in Structural Composites for Loading Monitoring and Damage Diagnostics

Dongfang Zhao <sup>1</sup>, Xingyu Liu <sup>2</sup>, Jacob Meves <sup>1</sup>, Christopher Billings <sup>1</sup> and Yingtao Liu <sup>1,\*</sup> 

<sup>1</sup> School of Aerospace and Mechanical Engineering, University of Oklahoma, Norman, OK 73019, USA; dongfang.zhao@ou.edu (D.Z.); jameves@ou.edu (J.M.); christopherbillings@ou.edu (C.B.)

<sup>2</sup> Oklahoma School of Science and Mathematics, Oklahoma City, OK 73104, USA; collins.liu@ossm.edu

\* Correspondence: yingtao@ou.edu; Tel.: +1-405-325-3663

**Abstract:** The development of novel embedded sensors for structural health monitoring (SHM) is crucial to provide real-time assessments of composite structures, ensuring safety, and prolonging their service life. Early damage diagnostics through advanced sensors can lead to timely maintenance, reducing costs and preventing potential catastrophic failures. This paper presents the synthesis, 3D printing, and characterization of novel embedded strain sensors using multi-walled carbon nanotube (MWCNT) -enhanced nanocomposites in fiberglass reinforced composites for potential damage diagnostics and SHM applications. MWCNTs are dispersed within structural epoxy for the additive manufacturing of nanocomposites with piezoresistive sensing capability. The 3D-printed nanocomposite sensors are embedded in fiberglass-reinforced composite laminates. The piezoresistive sensing capabilities of the 3D-printed sensors within composites are characterized by applying different levels of maximum loads and load rates under three-point bending loads. Additionally, the long-term reliability of the developed strain sensors is evaluated up to 1000 cycles. The recorded piezoresistive sensing signals show high sensitivity for the externally applied bending loads with advanced gauge factor up to 100, resulting in potential load sensing capability for in-situ damage diagnostics and real-time SHM for structural composites.

**Keywords:** composites; fiberglass; additive manufacturing; 3D printing; piezoresistive sensor; structural health monitoring; damage detection; direct ink writing



**Citation:** Zhao, D.; Liu, X.; Meves, J.; Billings, C.; Liu, Y. 3D Printed and Embedded Strain Sensors in Structural Composites for Loading Monitoring and Damage Diagnostics. *J. Compos. Sci.* **2023**, *7*, 437. <https://doi.org/10.3390/jcs7100437>

Academic Editors:  
Francesco Tornabene and Kun Fu

Received: 18 September 2023  
Revised: 10 October 2023  
Accepted: 12 October 2023  
Published: 14 October 2023



**Copyright:** © 2023 by the authors. Licensee MDPI, Basel, Switzerland. This article is an open access article distributed under the terms and conditions of the Creative Commons Attribution (CC BY) license (<https://creativecommons.org/licenses/by/4.0/>).

## 1. Introduction

Recent advances in structural composites have integrated nanotechnology and smart materials, leading to enhancements in strength, durability, and multifunctionality [1,2]. These cutting-edge structural composites are critical in diverse engineering applications, ranging from aerospace and automotive structures to renewable energy systems and next-generation civil infrastructures [3–6]. Although composites have demonstrated a broad range of benefits for practical applications, including high strength-to-weight ratio, improved corrosion resistance, high design flexibility, enhanced thermal stability, and reduced life-cycle costs, the early detection of damage in composites is still a significant challenge that should be addressed urgently [7,8]. Traditional materials, such as metal alloys, show visible signs of fatigue and fractures. However, damage in structural composite laminates, including micro-cracks, delamination, fiber brokage, and fiber pull-out, is often embedded under the composite surface, evading detection until they culminate in catastrophic failures.

Novel structural composites with embedded damage-sensing mechanisms present an exciting approach to address this challenge [9–11]. These embedded sensors and networks can allow certain structural composites to monitor their own structural health conditions and provide real-time feedback on their structural integrity. This self-sensing property not only prolongs the life of the composites but also ensures the safety of the entire composite structures and systems. Such innovations can lead to significant reductions in maintenance

costs, while also minimizing downtime and extending the overall service life of composite structures. Additionally, the potential integration of damage sensing capability using advanced sensors and sensing networks within the composite laminates has led to the development of complex structural health monitoring (SHM), damage diagnostics, and prognostics research in the last two decades [12–14]. A broad range of sensors, including acoustic sensors, fiber Bragg grating (FBG) fiber optic sensors, and piezoelectric sensors, have been employed for damage detection in structural composite laminates [15–18]. For example, Guo et al. used FBG fiber optic sensors for load monitoring and damage detection [19]. Yu et al. employed piezoelectric wafer sensors for damage detection and SHM in composite laminates using in-situ ultrasonic-guided wave analysis [20]. Liu et al. developed piezoelectric sensor arrays and time-frequency analysis for the guided Lamb wave for impact damage detection in composite laminates [21]. Additionally, time-frequency domain analysis for advanced signal processing was employed to comprehensively study the features in ultrasonic signals and potential damages that were represented by certain sensor signal features. Many of the reported sensors, including FBG and piezoelectric wafers, have been integrated as sensor arrays and embedded within structural composite laminates for SHM and real-time damage state awareness applications [22–25]. However, many challenges are still limiting the broad applications of embedded sensor-based SHM for broad engineering applications. Therefore, significant efforts are still urgently needed to solve challenges, including the potential degradation of composite properties caused by embedded sensors, short sensor durability, weak interface between sensors and composites, size and weight concerns, shortage of power supplies, and reliability and calibration requirements.

The development of smart materials and nanocomposites has enabled novel solutions to integrate self-sensing materials as embedded sensors in structural composites. Conductive nanoparticles, such as gold nanowires, silver nanowires, and multi-walled carbon nanotubes (MWCNTs) can be applied to the development of self-sensing composites reinforced by continuous structural fibers and fabrics. Abot et al. reported the synthesis and development of MWCNT thread in self-sensing composites [26]. MWCNT forests were spun into threads and integrated into composites as a sensor to monitor strains and detect damage, including delamination. Another approach was to synthesize novel structural polymers with color-changing capabilities and use the developed polymer as the matrix system in fiber-reinforced composites. Once external loads were applied, chemical reactions were triggered, and potential damage could be displayed as different colors on composite surfaces. For example, Zou et al. incorporated cyclobutane-containing cross-linked polymers into an epoxy matrix and demonstrated the impact damage monitoring capability by detecting fluorescence emission in glass fiber-reinforced composites [27]. Although novel polymers and nanocomposites provided unique sensing features for damage detection and SHM in composites, certain composite structures and components were fabricated using traditional wet-layup or autoclave curing. Precise sensor fabrication and embedment within composites are still needed to further broaden the application of certain novel polymers and nanocomposites.

Additive manufacturing (AM), also known as 3D printing, has emerged as a potent fabrication technique in the development of embedded sensors within composites. AM technologies allow the accurate control of the fabrication process, enabling the generation of intricate sensors with high spatial resolution directly into composites. A broad range of polymer AM technologies, such as fused deposition modeling (FDM), stereolithography (SLA) and digital light processing (DLP), and direct ink writing (DIW), have been employed for the in-situ manufacturing of embedded sensors for structural composite applications [28,29]. FDM-based polymer AM technology is well-accepted for the 3D printing of thermoplastic-based nanocomposites with self-sensing capability [30]. SLA- and DLP-based polymer AM technologies are renowned for their high surface smoothness and geometrical accuracy when used for 3D printing of load sensors [31,32]. DIW-based polymer AM technology offers unparalleled versatility in terms of material selection, ranging

from conductive polymers to metallic or nanocomposite inks, enabling tailored electrical and mechanical properties for the embedded sensors [33]. Additionally, the precision and controllability of the DIW process also provide opportunities for multi-material 3D printing, allowing for the creation of advanced, multifunctional sensors with layered or gradient functionalities.

Once embedded sensors are developed and fabricated, it is crucial to comprehensively evaluate the performance of these sensors in composite laminates before real engineering applications. The comprehensive evaluation of sensor performance involves assessing both their sensing capabilities and their impact on the composite structure. Technical approaches include conducting mechanical tests, such as tensile, compressive, three-point bending, and fatigue tests, to determine if the embedded sensors affect the material's intrinsic properties. Additionally, using advanced techniques, such as digital image correlation, can help visualize stress concentrations or defects that might arise due to sensor integration. Monitoring the sensor's long-term stability and reliability under varying environmental conditions, such as temperature, moisture, and cyclical loading is also essential. Potential challenges in evaluation arise from the embedded nature of these sensors, making direct inspections challenging.

To solve the discussed technical challenges, novel 3D printed and embedded strain sensors within continuous fiber-reinforced composites are reported in this paper. The nanocomposites, composed of MWCNTs and novel epoxy, were first developed, prepared, and employed for the 3D printing of embedded strain sensors. To obtain the appropriate rheological properties, two curing agents were combined for the viscosity optimization for structural epoxy. To the best of our knowledge, this is the first time that epoxy has been optimized using the developed curing agents for DIW-based 3D printing applications. Additionally, MWCNTs were uniformly dispersed within structural epoxy using shear force mixing. The prepared nanocomposites were 3D printed into the designed pattern on a composite lamina. Due to the superior electrical and mechanical properties of MWCNTs, the printed sensors obtained great piezoresistive load sensing capabilities with high sensitivity. Then, structural composite laminates were fabricated using traditional wet-up methods. The mechanical properties and MWCNT distributions in the fabricated composites were experimentally studied under three-point bending and cyclic loads to study the sensors long-term performance. Various applied load ranges and external load rates were employed to fully understand the sensor performance under complex load conditions.

## 2. Materials and Methods

### 2.1. Materials

Unless otherwise stated, all materials and reagents were used as received. The epoxy resin Epon 862 (diglycidyl ether of bisphenol F), curing agent Epikure W, and curing agent Epikure 9553 were purchased from Hexion, Columbus, OH, USA. The MWCNTs with diameters of 50–90 nm and an aspect ratio of 100 were purchased from Sigma Aldrich, Burlington, MA, USA. Fiberglass fabric tape with 1 in. width was purchased from Fiberglast.

### 2.2. Material Preparation and DIW-Based 3D Printing

The concentration of 1.5 wt.% MWCNTs were dispersed in the epoxy resin Epon 862 for the preparation of the 3D printable nanocomposites that could be processed using the DIW-based AM process. The MWCNTs were uniformly dispersed within the epoxy resin by mixing the two materials in a planetary Thinky AR100 mixer (Thinky USA, Laguna Hills, CA) for 10 min. Then, the two curing agents were hand mixed for two minutes at a 1:1 molecular ratio, then added to the mixed MWCNT/epoxy, and mixed again in the planetary Thinky AR100 mixer for five minutes to ensure the nanoparticles and epoxy materials were fully integrated. The mixture was loaded into a syringe and placed into a centrifuge for mixing and degassing for five more minutes. The mixed nanocomposite was transferred into a 10 cc syringe and loaded onto an in-house developed pneumatic-driven

DIW printer. The printer was modified to accommodate the nanocomposites, and a 25 gauge dispense nozzle tip was used for the print.

A fiberglass fabric tape (6 in. long and 1 in. wide) was attached to the build plate of the DIW 3D printer, and the nanocomposite was printed directly onto the center of the tap, with a constant pressure of 20 psi. After the print, two pieces of copper wire were planted into the electrodes at each end of the strain sensor, which was then allowed to solidify overnight at room temperature. Pristine Epon 862 resin and the same mixture of two curing agents were mixed for the wet layup of composite laminates without MWCNT. The layer with a 3D-printed nanocomposite sensor was used as the top layer and five additional layers of fiberglass fabric were stacked up using the wet layup process. Therefore, the 3D-printed strain sensor was placed between the first and second layers and embedded within the composite laminate. Since the maximum interlaminar stress was generated near the surface of composite laminates, the sensor location could allow the measurement of maximum stress in composites under three-point bending loads. The final composite laminates were pressurized using a vacuum bagging process at room temperature for eight hours and post-cured at 180 °C for two more hours. The final thickness of the composite was 2.2 mm ± 0.2 mm. Once fully cured, the sample was tested for the characterization of its mechanical and piezoresistive sensing capabilities. The schematic of material preparation, 3D printing, and composite fabrication process is shown in Figure 1. Figure 2a shows the manufactured composite laminate samples with embedded nanocomposite strain sensors.

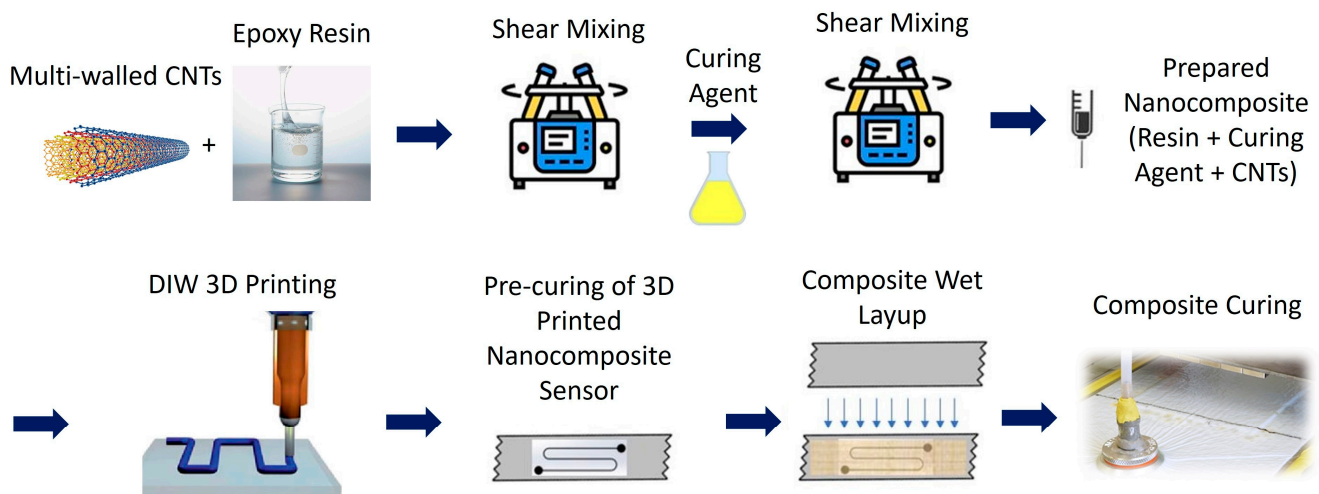


**Figure 1.** Schematic of material preparation, 3D printing, and composite fabrication processes.

### 2.3. Characterization of Piezoresistive-Based Sensing Capability

An Instron 5969 mechanical testing system was utilized for the characterization of the piezoresistive sensing capability of the 3D printed and embedded strain sensors in composite laminates under a three-point bending load, following the ASTM D790 standard.

Studying composite performance under three-point bending was essential to gain insights into their flexural behavior and mechanical properties under bending loads. Such tests replicated real-world conditions, providing valuable data on how the composite responded to bending stresses and strains. The flexural strain was calculated using the experimental data recorded using the Instron system following the equation below:

$$\varepsilon_f = 6Dd/L^2 \quad (1)$$

where  $\varepsilon_f$  is the flexural strain, D is the maximum deflection of the center of the beam, L is the support span length, and d is the thickness of the composite sample.

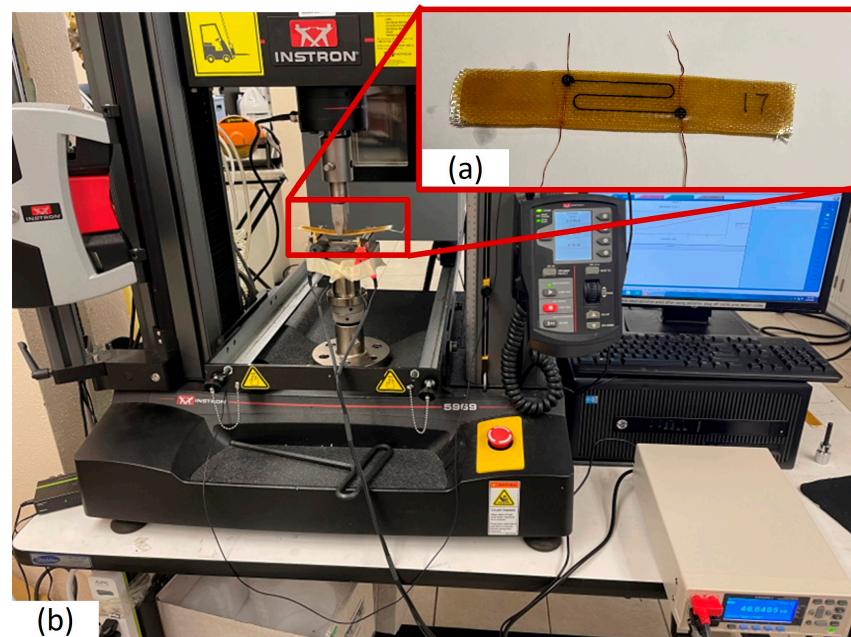


**Figure 2.** (a) Manufactured fiber glass reinforced composites with embedded MWCNT and epoxy nanocomposites as strain sensors for load sensing and damage detection; (b) experimental setup of piezoresistive sensor testing under three-point bending.

To record the change in resistance during the test, a HIOKI resistance meter was connected to the copper wires that extended out of the composite sample. The piezoresistive sensing signals were continuously recorded during the entire mechanical tests. To determine the appropriate load range, a sample was first tested until failure to determine the maximum applicable load, which was identified to be 210 N. Since the long-term sensor performance should be fully understood in this study, we decided to choose the maximum load of 35 N, 70 N, 105 N, and 140 N for cyclic tests and sensor characterization. Additionally, different strain rates were also employed to fully understand the effect of the applied strain rate on the piezoresistive sensing performance. Moreover, we studied the long-term sensor performance under cyclic loading conditions up to fatigue 1000 cycles. Figure 2b shows the experimental setup of the three-point bending using the Instron system and the HIOKI resistance meter.

#### 2.4. Microstructural Characterization Using Scanning Electron Microscopy

The ThermoFisher Quattro scanning electron microscope (SEM) was used to characterize the MWCNT distribution within the 3D-printed strain sensor. Multiple SEM images were taken under various magnitudes, showing the uniform dispersion of MWCNTs and conductive network formed by the introduced nanoparticles within epoxy, resulting in the piezoresistive sensing capability. Additionally, the fractured area of the composites after mechanical testing was also studied to understand the failure mode and evaluate the quality of the manufactured composites. Due to the low electrical conductivities of epoxy and fiberglass fabrics, the composite surfaces were sputter coated to avoid potential electric charge buildup on the sample surface in SEM.

### 3. Results and Discussion

#### 3.1. Evaluation of MWCNT Dispersion and Fracture in Composites

Uniform MWCNT dispersion was critical to create reliable piezoresistive sensing capability in the 3D-printed nanocomposite sensors. Due to the high surface area per unit volume of MWCNTs, these nanoparticles were intended to cause strong attractive interactions among them, resulting in a high tendency for aggregation and agglomeration. However, shear mixing of MWCNTs within epoxy enabled the dispersion of nanocompos-

ites and avoided potential agglomeration. Additionally, the shear force generated during the DIW 3D printing process was also able to disperse MWCNTs and align them along the printing direction, leading to enhanced piezoresistive sensing performance. Figure 3a,b demonstrate the uniform MWCNT dispersion in epoxy at the magnification of 2500 $\times$  and 12,000 $\times$ , respectively. No obvious agglomeration was observed during the SEM imaging. It is noted that a significant amount of MWCNTs were in contact with each other, resulting in measurable local contact resistance. Once deformed under applied strains, any potential sliding between adjacent MWCNTs would cause a change of local contact resistance. It is also noted that some MWCNTs were close to each other but did not have any physical contact. The tunnelling effect would be the sensing mechanism in this case. Any distance changes between adjacent MWCNTs would result in changes in the tunneling resistance. The combination of the changes in contact resistance and tunneling resistance resulted in the overall change of electrical resistivity in nanocomposites under applied strain, resulting in measurable piezoresistance sensing signals for strain measurement and potential damage diagnostics in composites.

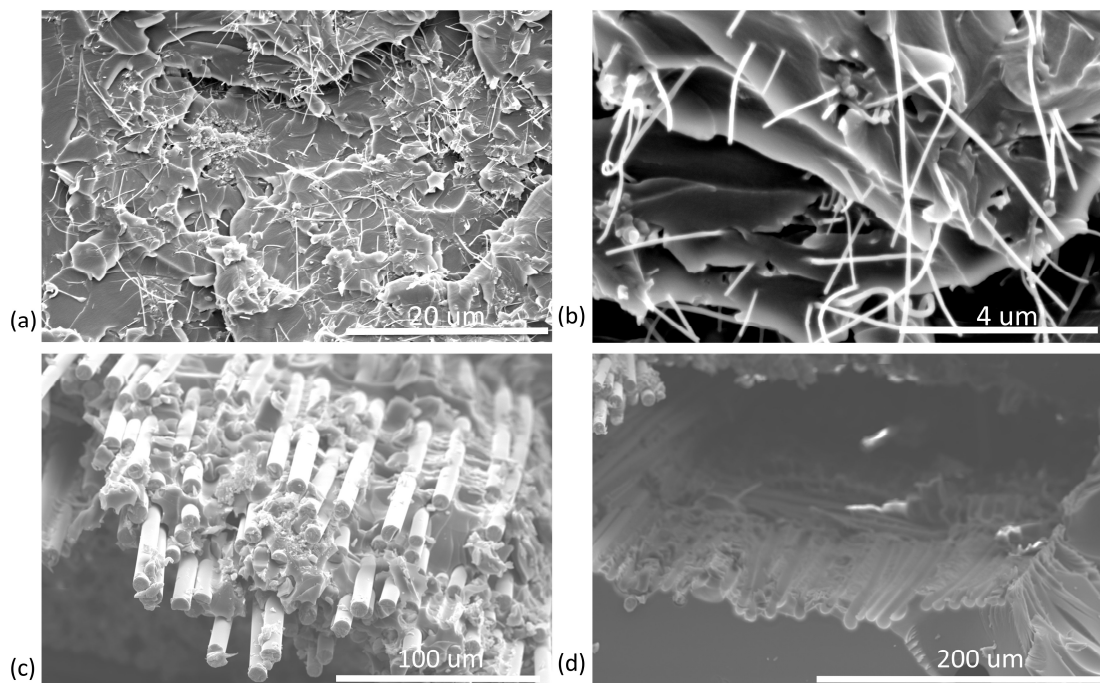


**Figure 3.** SEM images of embedded strain sensors and composites: (a,b) MWCNT distribution on the surface of 3D-printed nanocomposite sensors; (c) fiber pull-out on fractured surface of composite laminate; and (d) a socket left in composite matrix after fiber pull-out.

The employed composite manufacturing method has resulted in high-performance laminates. Figure 3c shows the fiber pull-out from the epoxy matrix in composites after fracture. This failure mode indicated that the main energy-absorbing mechanism raising the toughness of fiberglass composites was the pulling of fibers out of their sockets in the matrix during crack formation. Fracture energy was dissipated to a larger area during fiber pull-out. This toughening mechanism was beneficial in preventing catastrophic failure in composite laminates. Figure 3d shows the typical socket left in the epoxy matrix after a fiber pull-out. It is also worth noting that excessive fiber pull-out should be avoided for high-tensile strength composites by enhancing the fiber-matrix interface and increasing the degree of bonding between the fiber and the matrix in composites.

### 3.2. Piezoresistive Sensing under Quasi-Static Loads

The performance of the 3D printed and embedded strain sensors was first characterized under quasi-static loads. Composite beam samples were tested under three-point bending loads at the load rate of 10 mm/min and up to four maximum applied loads of 35 N, 70 N, 105 N, and 140 N. Figure 4a illustrates the piezoresistive sensing responses under these specified loads. Notably, all measured signals exhibited both a high signal-to-noise ratio and consistent repeatability. At the lower end, a maximum load of 35 N yielded minimal strain, leading to subdued piezoresistive sensing outputs. However, as the applied load intensified, there was a corresponding amplification in the sensor signals. The applied loads are shown in Figure 4b.

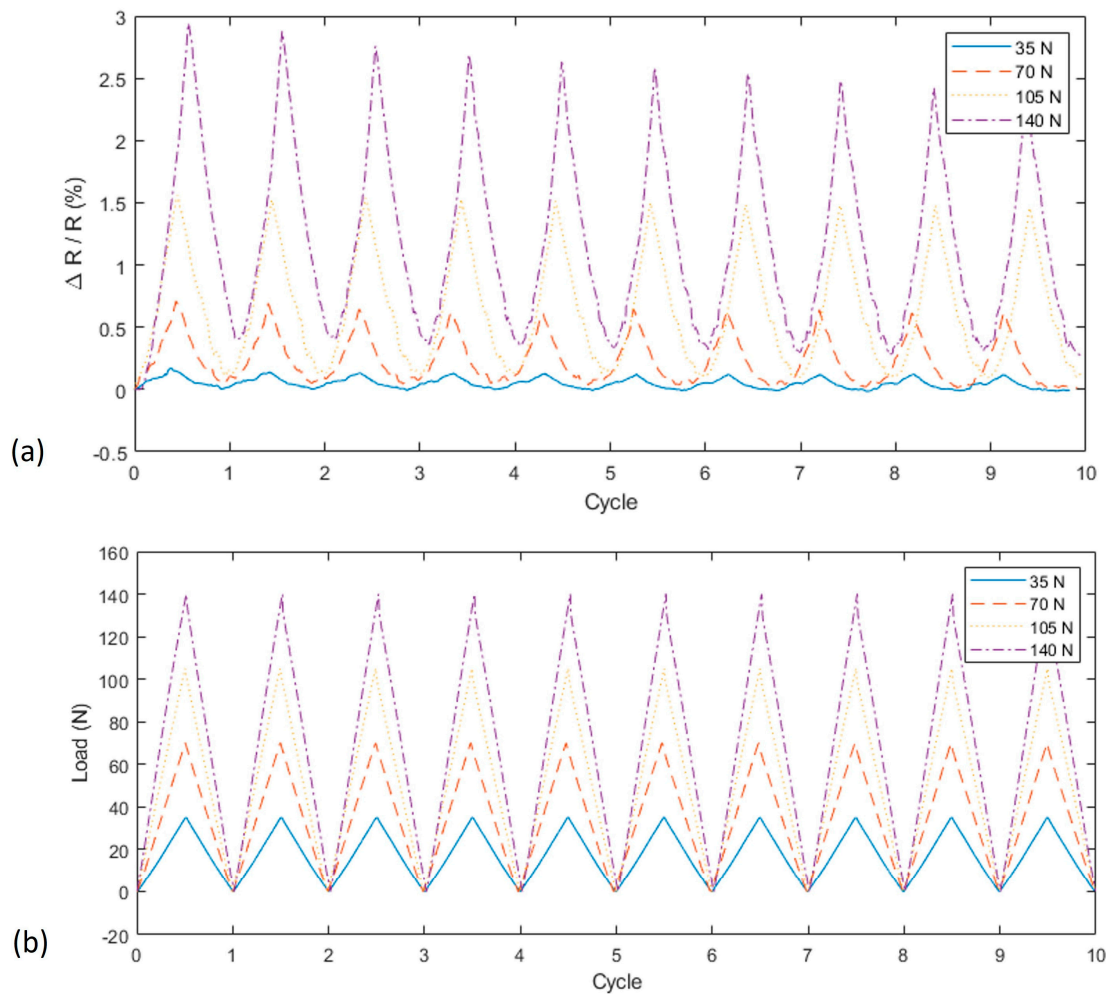


**Figure 4.** (a) Piezoresistive sensing signals under three-point bending cyclic loads with four levels of maximum forces of 35 N, 70 N, 105 N, and 140 N; (b) applied cyclic loads.

In the realm of strain sensing, the gauge factor (GF) stands as a paramount parameter to quantify a sensor’s sensitivity. Essentially, the gauge factor is defined as the relative change in electrical resistance for a given strain, mathematically expressed as:

$$GF = (\Delta R/R) / \epsilon_f \tag{2}$$

where  $\Delta R$  represents the change in resistance,  $R$  is the initial resistance, and  $\epsilon_f$  is the applied flexural strain calculated following the ASTM D790 standard in this paper.

The GFs of the reported nanocomposite sensor are shown in Table 1. It is noted that the measured GFs were in the range of 25–103, while traditional metal strain gauges have

the typical GF of 2–4 [34]. The significant increases in GF of 3D-printed nanocomposites are primarily due to the unique nanoscale interactions of MWCNTs, tunneling effects, and the reconfiguration of these nanofillers within the epoxy matrix in composites under the applied strains. Recognizing and understanding the GF is crucial, as it offers insights into the sensitivity and potential applications of the nanocomposite-based strain sensors in advanced technological domains.

**Table 1.** Calculated GF of embedded nanocomposite sensor in composite laminate.

Applied Maximum Load (N)	35	70	105	140
GF	26	45	87	103

### 3.3. Characterization of Load Rate Effects on Piezoresistive Sensing Capability

It has been reported that the performance of piezoresistive-based strain sensors can depend on external parameters, such as the applied load rate [35,36]. In this paper, the research team investigated how the applied three-point bending load rate can impact on the sensitivity of the piezoresistive sensing signals. Three different levels of applied load rates, including 1 mm/min, 10 mm/min, and 20 mm/min, were applied up to 105 N maximum applied load. As shown in Figure 5, there were obvious differences in the piezoresistive signals. The peak of the piezoresistive signal variation  $\Delta R/R$  under the three load conditions was about 1%, 1.5%, and 3.5%. Since the GF of the piezoresistive sensors were linearly correlated to the piezoresistive signal variation  $\Delta R/R$ , the GFs of the same nanocomposites depended on the applied load rates. Therefore, the sensitivity and related GF were different at these three loading conditions. This experimental study revealed that the piezoresistive sensing capability of nanocomposite sensors exhibited a distinct dependence on the load rate. Specifically, at rapid load rates, the sensors tended to demonstrate higher sensitivity owing to the more pronounced reconfiguration and realignment of MWCNT nanofillers within the polymer matrix. This heightened sensitivity resulted in a more pronounced change in the electrical resistance of the sensor for a given amount of strain. Conversely, at slower load rates, the rearrangement of nanofillers was more gradual, potentially leading to a diminished change in electrical resistance and, consequently, reduced sensitivity. Understanding this relationship is crucial for optimizing sensor performance in real-time applications and tailoring sensor responses to specific mechanical stimuli.

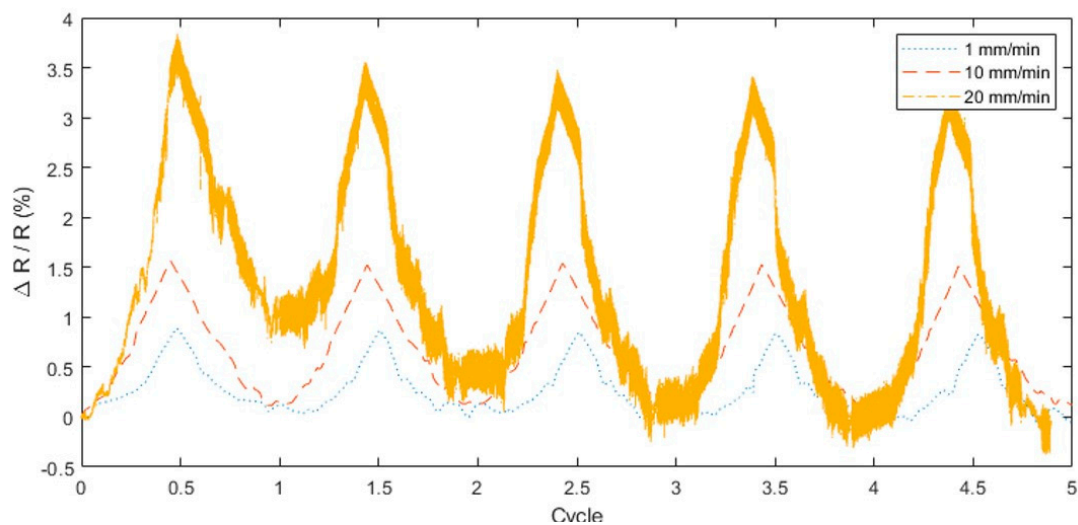


**Figure 5.** Piezoresistive sensor performance under various levels of applied load rates.

### 3.4. Characterization of Long-Term Piezoresistive Sensing Performance

To understand the embedded sensor durability and long-term performance, multiple cyclic tests were conducted and the piezoresistive sensor signals were recorded throughout all the tests. Since the embedded sensors were designed for SHM and damage diagnostic applications, it is imperative that their operational lifespan surpasses the designed life of the composites. Therefore, it is critical to evaluate how the embedded sensors would perform under a high number of cyclic tests. Highly reliable sensors could not only significantly reduce operational and maintenance costs, but also improve structural safety and integrity.

Figure 6 shows the sensor performance up to 100 cycles with a maximum load of 105 N. Throughout this test, the peak-to-valley values of each piezoresistive signal cycle remained consistent. However, there was a slight reduction in the maximum and minimum electrical resistance, potentially due to the realignment of MWCNTs during the cyclic tests. The consistent peak-to-valley sensor signals indicated the highly repeatable and reliable load-sensing capabilities of the embedded sensors within composite laminates.

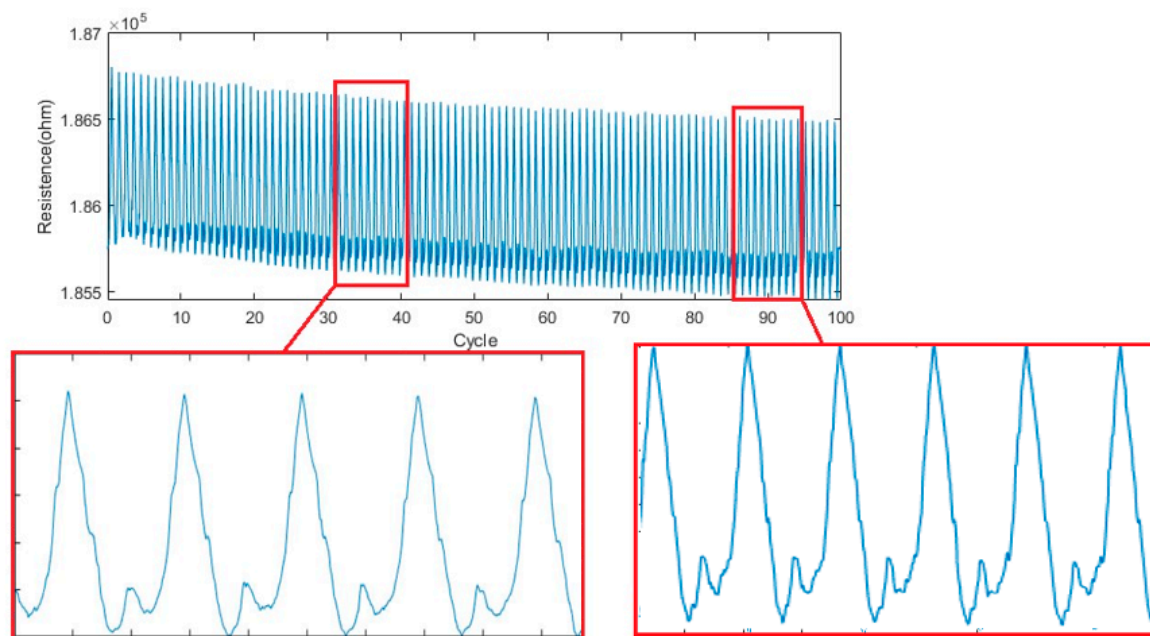


**Figure 6.** Piezoresistive sensor performance under three-point bending loads up to 100 cycles.

The 1000-cycle cyclic tests were conducted to further investigate the long-term performance of the embedded nanocomposite sensors in composite laminates. The typical sensor performance is shown in Figure 7. It is noted that the peak-to-peak piezoresistive sensing signal also remained consistent throughout these long-term tests. However, the maximum and minimum electrical resistance dropped in the first 100 cycles, but the reduction rate was visibly slowed later. The consistent peak-to-valley electrical resistance proved a strong proof of the robustness of the embedded sensor in cyclic load tests. It is reasonable to conclude that piezoresistive sensing single can still be a reliable indicator of the material's loading conditions. Once the measured load overpasses the allowed load levels, these sensor signals can be potential representations of any damage in composites for SHM analysis.

After undergoing long-term testing of 1000 cycles, the composite samples were further examined. Remarkably, even after these extensive tests, the samples could be tested for additional 100-cyclic tests without showing any significant signs of wear or degradation. The sensor performance was similar to the results reported in Figure 6. This resilience of the tested composite laminates with embedded sensors underscores the robust nature of the developed piezoresistive strain sensors, highlighting its potential for reliable service for SHM and damage diagnostics of structural composite applications and prolonged usage.

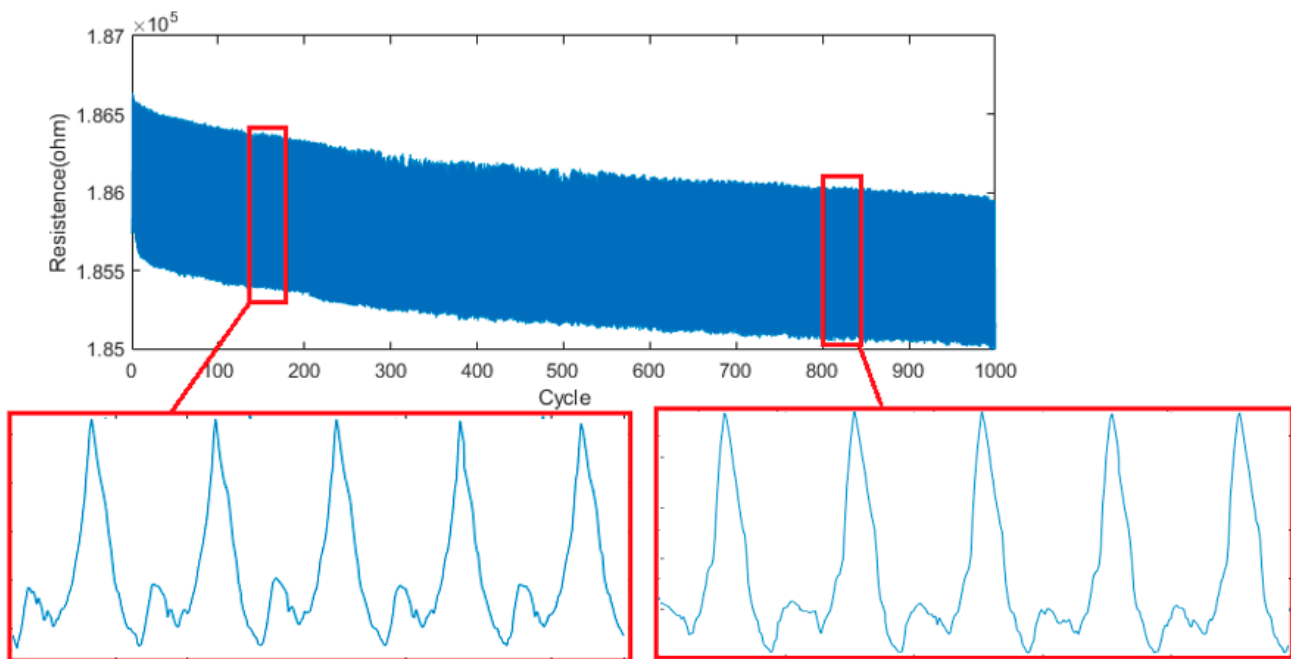


**Figure 7.** Piezoresistive sensor performance under three-point bending loads up to 1000 cycles.

#### 4. Conclusions

This paper reported the development of 3D printed and embedded strain sensors for load monitoring in composite laminates for potential damage detection and SHM applications. The 3D printable nanocomposite ink was developed by dispersing MWCNTs with a novel structural epoxy with a unique mixture of two curing agents. The developed nanocomposites showed both high 3D printability and an appropriate processing time window for material processing and curing. The 3D-printed nanocomposite strain sensors were embedded within fiberglass fabrics reinforced composite laminates, and the piezoresistive sensor performance was tested under cyclic loads with the maximum loads of 35 N, 70 N, 105 N, and 140 N, and three load rates of 1 mm/min, 10 mm/min, and 20 mm/min. The experimental results demonstrated the highly repeatable piezoresistive sensing capability of the embedded sensors. The high sensor reliability was demonstrated in cyclic fatigue tests up to 1000 cycles. It is worth noting that the developed embedded sensors demonstrated exceptionally high sensitivity, achieving a maximum gauge factor exceeding 100. This study indicated the potential damage monitoring and load sensing capabilities using 3D printed and embedded nanocomposite strain sensors within structural composites for SHM applications.

Regarding the future research directions, the reported work can be improved by enhancing sensor sensitivity and repeatability by exploring novel nanomaterials, like 2D materials or hybrid nanostructures, that might offer superior piezoresistive properties. Besides the reported self-sensing capability, additional nanocomposite functionalities, such as self-healing and self-powered sensors, can further increase the longevity and reliability of SHM systems. Integrating advanced data analytics and machine learning can also advance real-time damage detection and prediction, leading to the development of intelligent and adaptive composite structures. As the push towards more sustainable and intelligent infrastructure grows, these research directions are vital for the evolution of SHM applications.

**Author Contributions:** Conceptualization, Y.L. and D.Z.; validation, X.L., J.M., C.B. and Y.L.; formal analysis, D.Z.; writing—original draft preparation, D.Z.; writing—review and editing, Y.L.; supervision, Y.L. All authors have read and agreed to the published version of the manuscript.

**Funding:** This research was partially funded by the Oklahoma Aerospace and Defense Innovation Institute (OADII) and the Data Institute for Societal Challenges (DISC), Office of the Vice President for Research and Partnerships, University of Oklahoma.

**Data Availability Statement:** The data that support the findings of this study are available on request from the corresponding author, Yingtao Liu.

**Conflicts of Interest:** The authors declare no conflict of interest. The funders had no role in the design of the study; in the collection, analyses, or interpretation of data; in the writing of the manuscript; or in the decision to publish the results.

## References

1. Narayana, K.J.; Burela, R.G. A review of recent research on multifunctional composite materials and structures with their applications. *Mater. Today Proc.* **2018**, *5*, 5580–5590. [[CrossRef](#)]
2. Gibson, R.F. A review of recent research on mechanics of multifunctional composite materials and structures. *Compos. Struct.* **2010**, *92*, 2793–2810. [[CrossRef](#)]
3. Feldman, D. Polymer nanocomposites in building, construction. *J. Macromol. Sci. Part A* **2014**, *51*, 203–209. [[CrossRef](#)]
4. Su, Y.W.; Lin, W.H.; Hsu, Y.J.; Wei, K.H. Conjugated polymer/nanocrystal nanocomposites for renewable energy applications in photovoltaics and photocatalysis. *Small* **2014**, *10*, 4427–4442. [[CrossRef](#)] [[PubMed](#)]
5. Njuguna, J.; Pielichowski, K. Polymer nanocomposites for aerospace applications: Properties. *Adv. Eng. Mater.* **2003**, *5*, 769–778. [[CrossRef](#)]
6. Naskar, A.K.; Keum, J.K.; Boeman, R.G. Polymer matrix nanocomposites for automotive structural components. *Nat. Nanotechnol.* **2016**, *11*, 1026–1030. [[CrossRef](#)] [[PubMed](#)]
7. Galos, J. Thin-ply composite laminates: A review. *Compos. Struct.* **2020**, *236*, 111920. [[CrossRef](#)]
8. Abbas, S.; Li, F.; Qiu, J. A review on SHM techniques and current challenges for characteristic investigation of damage in composite material components of aviation industry. *Mater. Perform. Charact.* **2018**, *7*, 224–258. [[CrossRef](#)]
9. Okabe, Y.; Yashiro, S.; Kosaka, T.; Takeda, N. Detection of transverse cracks in CFRP composites using embedded fiber Bragg grating sensors. *Smart Mater. Struct.* **2000**, *9*, 832. [[CrossRef](#)]
10. Degrieck, J.; De Waele, W.; Verleysen, P. Monitoring of fibre reinforced composites with embedded optical fibre Bragg sensors, with application to filament wound pressure vessels. *Ndt E Int.* **2001**, *34*, 289–296. [[CrossRef](#)]
11. Huijter, A.; Kassapoglou, C.; Pahlavan, L. Acoustic emission monitoring of carbon fibre reinforced composites with embedded sensors for in-situ damage identification. *Sensors* **2021**, *21*, 6926. [[CrossRef](#)]
12. Giurgiutiu, V. *Structural Health Monitoring of Aerospace Composites*; Academic Press: Cambridge, MA, USA, 2015.
13. Liu, Y.; Nayak, S. Structural health monitoring: State of the art and perspectives. *Jom* **2012**, *64*, 789–792. [[CrossRef](#)]
14. Liu, Y.; Mohanty, S.; Chattopadhyay, A. Condition based structural health monitoring and prognosis of composite structures under uniaxial and biaxial loading. *J. Nondestruct. Eval.* **2010**, *29*, 181–188. [[CrossRef](#)]
15. Rocha, H.; Semprinoschnig, C.; Nunes, J.P. Sensors for process and structural health monitoring of aerospace composites: A review. *Eng. Struct.* **2021**, *237*, 112231. [[CrossRef](#)]
16. Giurgiutiu, V. SHM of aerospace composites—Challenges and opportunities. In Proceedings of the Composites and Advanced Materials Expo, Dallas, CA, USA, 27–29 October 2015; pp. 26–29.
17. Murukeshan, V.; Chan, P.; Ong, L.; Seah, L. Cure monitoring of smart composites using fiber Bragg grating based embedded sensors. *Sens. Actuators A Phys.* **2000**, *79*, 153–161. [[CrossRef](#)]
18. Tan, X.; Abu-Obeidah, A.; Bao, Y.; Nassif, H.; Nasreddine, W. Measurement and visualization of strains and cracks in CFRP post-tensioned fiber reinforced concrete beams using distributed fiber optic sensors. *Autom. Constr.* **2021**, *124*, 103604. [[CrossRef](#)]
19. Guo, H.; Xiao, G.; Mrad, N.; Yao, J. Fiber optic sensors for structural health monitoring of air platforms. *Sensors* **2011**, *11*, 3687–3705. [[CrossRef](#)] [[PubMed](#)]
20. Yu, L.; Santoni-Bottai, G.; Xu, B.; Liu, W.; Giurgiutiu, V. Piezoelectric wafer active sensors for in situ ultrasonic-guided wave SHM. *Fatigue Fract. Eng. Mater. Struct.* **2008**, *31*, 611–628. [[CrossRef](#)]
21. Liu, Y.; Fard, M.Y.; Chattopadhyay, A.; Doyle, D. Damage assessment of CFRP composites using a time–frequency approach. *J. Intell. Mater. Syst. Struct.* **2012**, *23*, 397–413. [[CrossRef](#)]
22. Lau, K. Structural health monitoring for smart composites using embedded FBG sensor technology. *Mater. Sci. Technol.* **2014**, *30*, 1642–1654. [[CrossRef](#)]
23. Qiu, Y.; Wang, Q.B.; Zhao, H.T.; Chen, J.A.; Wang, Y.Y. Review on composite structural health monitoring based on fiber Bragg grating sensing principle. *J. Shanghai Jiaotong Univ.* **2013**, *18*, 129–139. [[CrossRef](#)]
24. Aranguren, G.; Monje, P.; Cokonaj, V.; Barrera, E.; Ruiz, M. Ultrasonic wave-based structural health monitoring embedded instrument. *Rev. Sci. Instrum.* **2013**, *84*, 125106. [[CrossRef](#)] [[PubMed](#)]
25. Chia, C.C.; Jeong, H.M.; Lee, J.R.; Park, G. Composite aircraft debonding visualization by laser ultrasonic scanning excitation and integrated piezoelectric sensing. *Struct. Control Health Monit.* **2012**, *19*, 605–620. [[CrossRef](#)]
26. Abot, J.L.; Song, Y.; Vatsavaya, M.S.; Medikonda, S.; Kier, Z.; Jayasinghe, C.; Rooy, N.; Shanov, V.N.; Schulz, M.J. Delamination detection with carbon nanotube thread in self-sensing composite materials. *Compos. Sci. Technol.* **2010**, *70*, 1113–1119. [[CrossRef](#)]

27. Zou, J.; Liu, Y.; Shan, B.; Chattopadhyay, A.; Dai, L.L. Early damage detection in epoxy matrix using cyclobutane-based polymers. *Smart Mater. Struct.* **2014**, *23*, 095038. [[CrossRef](#)]
28. Jiang, Y.; Islam, M.N.; He, R.; Huang, X.; Cao, P.F.; Advincula, R.C.; Dahotre, N.; Dong, P.; Wu, H.F.; Choi, W. Recent advances in 3D printed sensors: Materials, design, and manufacturing. *Adv. Mater. Technol.* **2023**, *8*, 2200492. [[CrossRef](#)]
29. Sotov, A.; Kantyukov, A.; Popovich, A.; Sufiiarov, V. LCD-SLA 3D printing of BaTiO<sub>3</sub> piezoelectric ceramics. *Ceram. Int.* **2021**, *47*, 30358–30366. [[CrossRef](#)]
30. Andrew, J.J.; Alhashmi, H.; Schiffer, A.; Kumar, S.; Deshpande, V.S. Energy absorption and self-sensing performance of 3D printed CF/PEEK cellular composites. *Mater. Des.* **2021**, *208*, 109863. [[CrossRef](#)]
31. Arias-Ferreiro, G.; Lasagabáster-Latorre, A.; Ares-Pernas, A.; Ligeró, P.; García-Garabal, S.M.; Dopico-García, M.S.; Abad, M.-J. Lignin as a High-Value Bioadditive in 3D-DLP Printable Acrylic Resins and Polyaniline Conductive Composite. *Polymers* **2022**, *14*, 4164. [[CrossRef](#)]
32. Mahshid, R.; Isfahani, M.N.; Heidari-Rarani, M.; Mirkhalaf, M. Recent advances in development of additively manufactured thermosets and fiber reinforced thermosetting composites: Technologies, materials, and mechanical properties. *Compos. Part A Appl. Sci. Manuf.* **2023**, *171*, 107584. [[CrossRef](#)]
33. Armstrong, C.D.; Yue, L.; Kuang, X.; Roach, D.J.; Dunn, M.L.; Qi, H.J. A hybrid additive manufacturing process for production of functional fiber-reinforced polymer composite structures. *J. Compos. Mater.* **2023**, *57*, 841–850. [[CrossRef](#)]
34. Hoffmann, K. *An Introduction to Measurements Using Strain Gages*; Hottinger Baldwin Messtechnik Darmstadt: Darmstadt, Germany, 1989.
35. Abshirini, M.; Charara, M.; Liu, Y.; Saha, M.; Altan, M.C. 3D printing of highly stretchable strain sensors based on carbon nanotube nanocomposites. *Adv. Eng. Mater.* **2018**, *20*, 1800425. [[CrossRef](#)]
36. Chowdhury, S.A.; Saha, M.C.; Patterson, S.; Robison, T.; Liu, Y. Highly conductive polydimethylsiloxane/carbon nanofiber composites for flexible sensor applications. *Adv. Mater. Technol.* **2019**, *4*, 1800398. [[CrossRef](#)]

**Disclaimer/Publisher's Note:** The statements, opinions and data contained in all publications are solely those of the individual author(s) and contributor(s) and not of MDPI and/or the editor(s). MDPI and/or the editor(s) disclaim responsibility for any injury to people or property resulting from any ideas, methods, instructions or products referred to in the content.